deformation for ^{47}Ti. However, even if the known positive-parity states are omitted from the experimental level schemes, the observed level densities are still larger than those predicted by this model.

B. $T=\frac{5}{2}$ States

The isobaric analog state of the ^{49}Ti ground state should occur at 6.3–6.5-MeV excitation in ^{49}V. Since this transition carries little strength in the (^{3}He,d) reaction $[(2j+1)S=0.4]$ and is kinematically unfavored, it is not surprising that no candidate for such an assignment can be uniquely determined from among the levels of Table I. A comparison between the present data and the ^{48}Ti(d,p)^{49}Ti data of Ref. 7 reveals that the strong (^{3}He,d) transitions to states 76 (7783 keV) and 82 (8111 keV) may correspond to the strong $l=1$ transitions to ^{49}Ti states at 1384 and 1724 keV, respectively, observed in the (d,p) reaction. The (^{3}He,d) angular distributions are consistent with $l=1$ assignments and both transitions are among the strongest observed, as are the corresponding (d,p) transitions. The Coulomb energies corresponding to the two proposed $T=\frac{5}{2}$ states are shown in Table IV. It is characteristic that the (^{3}He,d) reaction in the energy range considered (6.4–8.7 MeV) excites, altogether, 42 states, compared to a total of eight (d,p) transitions in the corresponding ^{49}Ti range (0–2.3 MeV).

If the DW calculations are extrapolated from the bound to the unbound region, keeping the bound-state wave function fixed near zero binding, the estimated (^{3}He,d) strengths of the two $l=1$ transitions to the analog states (levels 76 and 82) are $\approx$0.4 and $\approx$0.15, respectively. The corresponding ^{48}Ti(d,p) strengths divided by $(2T+1)=5$ are 0.5 and 0.12, respectively.

ACKNOWLEDGMENTS

The authors wish to thank Professor R. Middleton and Professor W. E. Stephens for their continued interest in this work. It is a pleasure to acknowledge the help of Dr. R. H. Bassel in performing part of the distorted-wave analysis, and also P. Neogy, who assisted with the data analysis. The excellent service rendered by the NEUCC computing centre in Lundtofte, Denmark is greatly appreciated. The scanning of the nuclear emulsions was carefully performed by Mrs. M. Scrinivasan and Mrs. C. Coliukus.

PHYSICAL REVIEW VOLUME 166, NUMBER 4 20 FEBRUARY 1968

Distribution of Radionuclides from the Interaction of 3- and 29-GeV Protons with Silver*

SEYMOUR KATCOFF, HARRY R. FICKEL,† AND ARMIN WYTTENBACH‡
Chemistry Department, Brookhaven National Laboratory, Upton, New York
(Received 4 August 1967)

Formation cross sections have been measured of about 60 radionuclides isolated from Ag irradiated by 3- and 29-GeV protons. From these data, isobaric charge distributions and mass-yield curves were derived. At 3 GeV, the total isobaric cross sections are ~40 mb near the target, and they decrease to a broad minimum of 4 mb at around $A=30$–40. For lighter products the cross sections increase again. At 29 GeV, light- and intermediate-mass products ($20<A<50$) have 20–100% higher cross sections than at 3 GeV; the heavier products ($A>65$) have 10–20% lower yields. Corresponding charge-distribution curves at the two energies are identical except for shifts in absolute magnitude. Comparison of the 3-GeV mass-yield curve with the results of a Monte Carlo calculation based on a cascade-evaporation model shows that such a mechanism can account for the observed cross sections down to about mass 50. The lower-mass products ($15<A<35$) must be formed mainly in a fragmentation or "fission-like" process. Comparisons are made with previous nuclear-emulsion and radiochemical results.

INTRODUCTION

NUCLEAR reactions of high-energy particles with complex nuclei have been studied by a variety of techniques.[1,2] These involve the use of counters, nuclear emulsions, bubble chambers, mass spectrometry, and radiochemistry. The last two methods have been used to measure product cross sections from the reaction of GeV protons with various targets.[3–7] However, no complete

* Research performed under the auspices of the U. S. Atomic Energy Commission.
† Present address: Domtar Research Centre, Senneville, P. Q. Canada.
‡ Present address: Eidg. Institut für Reaktorforschung, Würenlingen, Switzerland.
[1] J. M. Miller and J. Hudis, Ann. Rev. Nucl. Sci. **9**, 159 (1959).
[2] J. Hudis, *High-Energy Nuclear Reactions, Nuclear Chemistry*, edited by L. Yaffe (Academic Press Inc., New York, 1967), Chap. 3.
[3] R. Wolfgang, E. W. Baker, A. A. Caretto, J. B. Cumming, G. Friedlander, and J. Hudis, Phys. Rev. **103**, 394 (1956).
[4] J. R. Grover, Phys. Rev. **126**, 1540 (1962).
[5] G. Rudstam and G. Sørensen, J. Inorg. Nucl. Chem. **28**, 771 (1966).
[6] G. Friedlander, *Physics and Chemistry of Fission* (International Atomic Energy Agency, Vienna, 1965), Vol. II, p. 265.
[7] J. Hudis, I. Dostrovsky, G. Friedlander, J. R. Grover, N. T. Porile, L. P. Remsberg, R. W. Stoenner, and S. Tanaka, Phys. Rev. **129**, 434 (1963).

TABLE I. Radioactive products studied, their detected radiations with abundances, and the methods of measurement.

Nuclide	Half-life	Radiation detected (Energy in keV)	Abundance	Remarks
Na^{22}	2.6 year	511 annih.	1.80	a, b
Na^{22}	2.6 year	1275 γ	1.00	a, b
Na^{24}	15 h	1370 γ	1.00	a, b
Mg^{28}	21.3 h	1780 γ (Al^{28})	1.00	a
P^{32}	14.3 day	1710 β^-	1.00	c
K^{42}	12.4 h	1520 γ	0.18	a
K^{43}	22 h	374+···+394 γ's	1.03	a, d
K^{43}	22 h	591+619 γ's	0.94	a, d
Ca^{45}	165 day	250 β^-	1.00	c
Ca^{47}	4.7 day	1310 γ	0.77	a, e
Sc^{43}	3.9 h	370 γ	0.215	a, d
Sc^{43}	3.9 h	511 annih.	1.76	a, f
Sc^{44}	4.0 h	1160 γ	1.00	a, d
Sc^{44m}	2.4 day	271 γ	0.90	a, g
Sc^{46}	84 day	890 γ	1.00	a, d
Sc^{46}	84 day	1120 γ	1.00	a, d
Sc^{47}	3.4 day	160 γ	0.70	a
Sc^{48}	44 h	1310 γ	1.00	a, h
Sc^{49}	57 min.	2010+···β^-	1.00	c
Ti^{45}	3.08 h	511 annih.	1.70	b
V^{48}	16.1 day	1310 γ	0.98	a, h
V^{49}	330 day	4.5 x rays	0.175	i, j
Cr^{48}	23 h	116 γ	0.98	a, d
Cr^{48}	23 h	305 γ	0.99	a, h
Cr^{49}	42 min.	1390+···+1540 β^+	0.93	c
Cr^{51}	28 day	320 γ	0.090	a
Mn^{52}	5.7 day	1430 γ	1.00	a, h
Mn^{54}	303 day	835 γ	1.00	a
Fe^{55}	2.6 year	5.9 x ray	0.257	c, i
Fe^{59}	45 day	270+460 β^-	1.00	c
Fe^{59}	45 day	1290 γ	0.44	a
Co^{55}	18 h	931 γ	0.73	a, f
Co^{56}	77 day	1240 γ	0.70	a, d
Co^{56}	77 day	1750 γ	0.18	a, h
Co^{56}	77 day	2600 γ	0.16	a, d
Co^{57}	267 day	122+136 γ's	0.96	a
Co^{58}	71 day	805+···+845 γ's	1.01	a, f, k
Co^{60}	5.26 year	1173 γ	1.00	l
Co^{60}	5.26 year	1332 γ	1.00	l
Co^{61}	1.65 h	68 γ	0.90	a
Cu^{61}	3.3 h	940+1220 β^+	0.62	c
Cu^{64}	12.9 h	570 β^-+660 β^+	0.57	c
Cu^{67}	61 h	400+···+570 β^-	1.00	c
Zn^{65}	245 day	1116 γ	0.50	a
Ga^{67}	79 h	185+209 γ's	0.30	a, f
Ga^{72}	14.1 h	835 γ	0.97	a
As^{71}	65 h	175 γ	0.91	a
As^{72}	26 h	835 γ	0.77	a, f
As^{73}	76 day	54 γ	0.090	a, m
As^{74}	17.7 day	596+635 γ's	0.76	a, f
Se^{72}	8.4 day	same as As^{72}		n
Se^{75}	120 day	265+280 γ's	0.77	a, f
Rb^{83}	83 day	521+···+553 γ's	0.93	a, o
Rb^{84}	33 day	880 γ	0.74	a, f
Sr^{82}	25 day	511 annih. (Rb^{82})	1.92	a, p
Sr^{83}	33 h	same as Rb^{83}		n
Sr^{85}	64 day	514 γ	0.99	a, p
Zr^{88}	85 day	394 γ	0.98	a
Zr^{89}	78.4 h	908 γ	1.00	a
Ru^{97}	2.85 day	220 γ	0.88	a
Ru^{103}	40 day	498 γ	0.88	a
Rh^{101}	3.2 year	198 γ	0.90	l
Pd^{100}	4.0 day	19 x ray	0.69	q, r
Pd^{101}	8.4 h	20 x ray	0.71	q, s
Pd^{103}	17 day	20 x ray	0.71	q, t
Ag^{103}	1.1 h	same as Pd^{103}		n
Ag^{105}	40 day	21 x ray	0.72	q, u
Ag^{106m}	8.3 day	21 x ray	0.72	q

[a] Counted with 3 in. ×3 in. NaI crystal.
[b] Counted in NaI well crystal.
[c] Counted with thin-window β-proportional flow counter.
[d] Correction between 1.11 and 1.20 applied for summing with other γ rays.
[e] Intensity of 160-keV γ ray of daughter Sc^{47} also measured and found in good agreement.
[f] Correction between 1.01 and 1.10 applied for summing with other γ rays.
[g] Intensity of 1160-keV γ also measured and found in good agreement.
[h] Correction between 1.21 and 1.30 applied for summing with other γ rays.
[i] Counted with argon-filled x-ray proportional counter, 4-in.-diam thin Be window.
[j] Large self-absorption corrections for soft x rays make V^{49} activity measurements uncertain by ±35%.
[k] Correction between 0.75 and 0.80 applied to subtract contribution of Co^{56}.
[l] Measured with Ge(Li) detector in old irradiated Ag foils without chemical separation.
[m] Abundance of 54-keV γ taken from Ref. 13.
[n] Parent isolated, daughter activity measured.
[o] Small correction applied to subtract counting rate of 511-keV annihilation radiation.
[p] 1.6 g/cm² copper absorber added for annihilation of β^+; absorption correction = 1.14.
[q] Counted with 2-mm thick NaI crystal and single-channel analyzer. Small corrections of ~5% each applied for self-absorption and absorption in beryllium.
[r] Correction for β^+ emission by Rh^{100} = 1.05.
[s] Correction for β^+ emission = 1.03; correction for K vacancy produced by 24-keV transition = 0.61.
[t] Correction for K vacancy produced by 53-keV transition = 0.96; correction for Rh^{103m} = 0.93.
[u] Correction for K vacancy produced by 64-keV transition = 0.90.

study has been made for any target from the middle of the periodic table. This would be especially useful because then it would be possible to make comparisons with the results of nuclear-emulsion experiments, where the target nuclei are Ag and Br.

For the present investigation silver was selected as the target and it was bombarded with both 3- and 29-GeV protons. About 60 product nuclides were isolated and measured at each energy. Information was obtained on isobaric charge distribution for products in various mass regions and mass-yield curves were obtained at both bombarding energies. The data are compared with the results of a Monte Carlo cascade-evaporation calculation, with nuclear-emulsion data, and with the results of similar radiochemical studies with other targets.

EXPERIMENTAL

Silver foils were irradiated in the circulating beams of the Brookhaven 3-GeV Cosmotron and the 30-GeV Alternating Gradient Synchrotron. A typical target stack consisted of two 27 mg/cm² Ag foils sandwiched between two 13 mg/cm² Ag guard foils, two 2 mg/cm² Al guard foils, and finally two 7 mg/cm² Al monitor foils. Irradiation times varied between 10 min and 8 h. About 1 cm² was carefully cut out with a razor blade from the most intensely irradiated portion of each stack. The 15-h Na^{24} in the Al monitor foils was counted several times with standardized β-proportional counters over a period of a few days. From the amount of Na^{24}, extrapolated to the end of irradiation time, the weight of the Al, and the known formation cross sections, the

TABLE II. Product cross sections from bombardment of silver with 3- and 29-GeV protons, and the corresponding ratios of cross sections, σ_{29}/σ_3. In the third column, (c) indicates cumulative yields when at least one of the precursors is known; (i) indicates independent yields. Values from individual runs are given in the first and last columns.

σ (3 GeV) (mb)	σ_3 (mean)	Nuclide	σ_{29}/σ_3	σ_{29} (mean)	σ (29 GeV) (mb)
	10[a]	He^6			
	4[b]	Li^8 (c)			
	1.05[c]	Li^9			
	8[d]	Be^7	2.3	18.2[d]	
	2.3[e]	C^{11}			
	0.176[c]	C^{16}			
	0.22[f]	N^{13} (c)			
	0.99[c]	N^{17}			
	1.43[g]	F^{18} (c)			
	6.5[h]	Ne^{20}(c)	2.31	15[h]	
	6.5[h]	Ne^{21} (c)	2.31	15[h]	
	6.1[h]	Ne^{22} (c)	2.25	13.7[h]	
	0.20[i]	Ne^{24}			
1.12, 1.15	1.14[j]	Na^{22} (c)	2.06	2.35[j]	2.35, 2.40, 2.29
2.33, 2.15	2.24[j]	Na^{24} (c)	1.83	4.10[j]	4.35, 4.05, 3.90
0.341, 0.321, 0.318	0.327[j]	Mg^{28}	1.82	0.594[j]	0.586, 0.628, 0.571, 0.590
2.37, 2.65	2.51[k]	P^{32} (i)			
	0.32[h]	Ar^{36}	1.47	0.47[h]	
	1.21[h,l]	Ar^{37} (c)	1.78	2.15[h,l]	
	4.7[h]	Ar^{38} (c)	1.49	7.0[h]	
	2.7[h,l]	Ar^{39} (c)	1.67	4.5[h,l]	
	0.41[l]	Ar^{41}	1.54	0.63[l]	
	0.12[h,l]	Ar^{42}	1.58	0.19[h,l]	
1.71, 1.64, 1.65	1.67[k]	K^{42} (i)	0.59	0.987[k]	0.978, 0.997
0.721, 0.666, 0.703	0.697[j]	K^{43}	0.66	0.462[k]	0.458, 0.465
0.677, 0.668, 0.835	0.727[m]	Ca^{45} (c)	1.53	1.12[m]	1.14, 1.08, 1.09, 1.18
0.049, 0.054	0.052[k]	Ca^{47} (c)	1.73	0.090[k]	0.089, 0.089, 0.099, 0.082
0.92, 0.84	0.88[m]	Sc^{43} (c)	1.34	1.18[m]	0.91, 1.43, 1.08, 1.31
0.84, 0.87	0.86[m]	Sc^{44} (i)	1.30	1.12[m]	1.22, 0.90, 1.19, 1.16
1.50, 1.46	1.48[k]	Sc^{44m} (i)	1.33	1.97[k]	1.77, 2.04, 2.09, 2.00
2.96, 3.27	3.12[k]	Sc^{46} (i)	1.10	3.44[k]	3.40, 3.49
1.76, 1.58	1.67[k]	Sc^{47} (i)	1.02	1.70[k]	1.83, 1.56, 1.73, 1.66
0.33	0.33[n]	Sc^{48} (i)	1.42	0.47[m]	0.48, 0.46, 0.49, 0.46
~0.12, ~0.09	~0.11[n]	Sc^{49} (c)	~1.3	~0.14[o]	~0.14
0.64, 0.68	0.66[k]	Ti^{45} (c)	1.50	0.99[k]	0.98, 0.99
1.99, 1.92, 2.19	2.03[k]	V^{48} (c)	1.37	2.78[k]	2.83, 2.70, 2.71, 2.87
3.30, 2.22, 2.42	2.64[o]	V^{49} (c)	2.39	6.3[o]	7.4, 5.1, 6.5
0.043, 0.046, 0.042, 0.049	0.045[k]	Cr^{48}	1.36	0.061[k]	0.059, 0.064
0.51	0.51[n]	Cr^{49}			
6.67, 5.76, 6.02, 7.50	6.49[m]	Cr^{51} (c)	1.10	7.15[m]	6.85, 7.55, 6.95, 7.25
2.47	2.47[n]	Mn^{52} (c)			
4.74, 5.20, 4.75	4.90[k]	Mn^{54} (i)	1.13	5.55[k]	5.64, 5.73, 5.28
4.31, 4.75, 4.34	4.47[k]	Fe^{55} (c)	1.15	5.16[k]	4.96, 5.44, 5.09, 5.13
0.466, 0.558, 0.531	0.52[k]	Fe^{59} (c)	1.21	0.626[k]	0.602, 0.665, 0.632, 0.604
0.237	0.237[n]	Co^{55}	0.87	0.207[k]	0.204, 0.210
~2.3	~2.3[o]	Co^{56}	~0.8	~1.8[o]	~1.8
4.16, 4.16, 4.66, 4.49, 4.26	4.35[k]	Co^{57} (c)	0.99	4.31[k]	4.61, 3.97, 4.27, 4.37
5.71, 6.05, 5.75, 5.98, 5.49	5.80[k]	Co^{58} (i)	0.95	5.51[k]	5.83, 5.04, 5.41, 5.51, 5.72
1.84, 1.94	1.89[k]	Co^{60} (i)	1.08	2.05[k]	2.13, 1.96
0.94	0.94[n]	Co^{61} (c)	0.94	0.88[k]	0.89, 0.87
3.56, 3.22, 2.94	3.24[m]	Cu^{61} (c)	0.84	2.72[m]	2.74, 2.71
4.36, 3.98, 3.92	4.09[m]	Cu^{64} (i)	0.87	3.57[m]	3.57, 3.57
0.250, 0.197	0.223[m]	Cu^{67} (c)	0.86	0.191[m]	0.190, 0.192
10.34, 10.36	10.35[k]	Zn^{65} (c)	0.84	8.71[k]	8.62, 8.70, 8.82, 8.70
8.45, 7.71	8.08[m]	Ga^{67} (c)	0.80	6.46[m]	6.63, 6.29
0.311, 0.253	0.282[m]	Ga^{72} (i)	0.93	0.261[k]	0.257, 0.264
8.09, 8.15	8.12[k]	As^{71} (c)	0.78	6.32[k]	6.24, 6.41
8.41, 8.15	8.28[k]	As^{72} (i)	0.80	6.66[k]	6.56, 6.76

TABLE II (*continued*)

σ (3 GeV) (mb)	σ_3 (mean)	Nuclide	σ_{29}/σ_3	σ_{29} (mean)	σ (29 GeV) (mb)
16.17, 16.27	16.2[k]	As^{73} (c)	0.80	12.9[k]	12.41, 13.35
3.09, 2.93	3.01[k]	As^{74} (i)	0.81	2.43[k]	2.39, 2.46
3.68, 3.18	3.43[k]	Se^{72}	0.72	2.47[k]	2.43, 2.51
20.1, 15.8, 21.8, 18.2	19.0[m]	Se^{75} (c)	0.71	13.5[k]	13.7, 12.4, 14.6, 13.2
	1.8[h,l]	Kr^{76}	0.78	1.4[h,l]	
	3.8[l]	Kr^{77}	0.89	3.4[l]	
	11.1[h]	Kr^{78}	0.80	8.9[h]	
	12.6[h,l]	Kr^{79} (c)	0.93	11.7[h,l]	
	16.6[h]	Kr^{80} (c)	0.80	13.2[h]	
	17.0[h]	Kr^{81} (c)	0.80	13.6[h]	
	17.7[h]	Kr^{82} (c)	0.80	14.1[h]	
	17.9[h]	Kr^{83} (c)	0.80	14.3[h]	
	1.83[h]	Kr^{84} (c)	0.85	1.55[h]	
	0.035[h]	Kr^{85} (c)	0.66	0.023[h]	
	1.14[l]	Rb^{79}	4.0	4.6[l]	
21.9, 22.1	22.0[j]	Rb^{83} (c)	0.69	15.1[j]	15.5, 14.8
5.01, 4.87	4.94[k]	Rb^{83} (i)	0.73	3.60[k]	3.71, 3.50
2.26	2.26[n]	Rb^{84} (i)	0.67	1.52[k]	1.50, 1.54, 1.51, 1.52
8.82, 8.18	8.50[m]	Sr^{82} (c)	0.75	6.36[m]	6.45, 6.70, 5.92
18.4, 17.9, 15.3	17.2[m]	Sr^{83} (c)	0.66	11.38[m]	11.31, 11.45
19.5	19.5[n]	Sr^{85} (c)	0.81	15.8[k]	15.8, 15.4, 16.3
20.6, 19.6	20.1[k]	Zr^{88} (c)	0.76	15.2[k]	15.1, 15.4
23.1, 22.1	22.6[k]	Zr^{89} (c)	0.77	17.5[k]	17.3, 17.7
20.9, 18.0	19.5[k]	Ru^{97} (c)	0.98	19.1[n]	19.1
0.83, 0.78	0.81[k]	Ru^{103} (c)	1.14	0.92[k]	0.88, 0.83, 0.95, 1.03
3.20, 3.28	3.24[m]	Rh^{101}	0.89	2.89[m]	3.31, 2.98, 2.38
7.19, 5.97, 6.85	6.67[m]	Pd^{100} (c)	0.84	5.63[m]	5.32, 5.93
16.0, 15.5, 17.1	16.2[m]	Pd^{101} (c)	0.83	13.4[m]	13.2, 13.7
25.7, 26.0, 27.8, 29.7	27.3[k]	Pd^{103} (c)	0.95	25.9[k]	25.4, 26.3
18.4	18.4[n]	Pd^{103} (i)	0.97	17.8[m]	17.3, 18.2
9.6, 9.7, 9.4	9.6[m]	Ag^{103} (c)	0.84	8.08[m]	8.43, 7.73
31.4, 28.4, 29.9, 30.8	30.1[k]	Ag^{105} (c)	0.94	28.4[k]	28.8, 27.9, 28.5, 28.3
12.3, 11.7, 12.2, 13.5	12.4[k]	Ag^{106} (i)			

[a] F. S. Rowland and R. L. Wolfgang, Phys. Rev. **110**, 175 (1958).
[b] S. Katcoff, Phys. Rev. **164**, 1367 (1967); also S. Katcoff, E. W. Baker, and N. T. Porile, *ibid.* **140**, B1549 (1965).
[c] Reference 23.
[d] E. Baker, G. Friedlander, and J. Hudis, Phys. Rev. **112**, 1319 (1958); J. Hudis (private communication).
[e] R. Sharp (private communication).
[f] I. Dostrovsky, Z. Fraenkel, and J. Hudis, Phys. Rev. **123**, 1452 (1961).
[g] A. A. Caretto, Jr., J. Hudis, and G. Friedlander, Phys. Rev. **110**, 1130 (1958).
[h] Reference 31.
[i] J. Hudis (private communication).
[j] Estimated accuracy of mean, ±10%.
[k] Estimated accuracy of mean ±15%.
[l] Reference 32.
[m] Estimated accuracy of mean, ±20%.
[n] Estimated accuracy of mean, ±25%.
[o] Estimated accuracy of mean, ±35%.

proton flux could be calculated. The Na^{24} cross sections[8] used were 9.1 mb for 3 GeV and 8.6 mb for 29 GeV. Small corrections of about 2–3% were needed to correct for recoil loss and secondary effects. The leading edges of the foils were included but in order to minimize errors due to imperfect lineup of the foils, both forward and aft monitors were measured. In all runs the activities in both monitors agreed to within a few percent, usually $\leqslant 3\%$.

The irradiated silver foils were weighed and then dissolved in $4N$ HNO_3 containing 5–20 mg carrier of each of the elements to be determined in a particular run. Usually two to four elements were isolated, in duplicate, in each run. For the most part, standard radiochemical procedures[9,10] were used. Most of the activity measurements were by means of γ-ray spectroscopy with a 3-in.×3-in. NaI detector and a multichannel analyzer. A few of the later measurements were also done with a Ge(Li) detector. Selected γ-ray photopeaks were measured as a function of time, so that most of the radionuclides were characterized both by means of their γ-ray energies and half-lives. The counters were calibrated with standard sources from the National Bureau of Standards. Table I lists the product nuclides that were measured, the radiations which were selected

[8] J. B. Cumming, Ann. Rev. Nucl. Sci. **13**, 261 (1963).

[9] *Radiochemistry Monographs*, NAS-NS 3001 to NAS-NS 3058 (Office of Technical Services, Department of Commerce, Washington, D. C., 1961–67).

[10] The radiochemical analyses for Cr isotopes gave reproducible results only when reduction of chromium from the +6 valence state to +2 was included in the procedure.

for measurement, the detectors used, and the important corrections. Branching ratios, half-life values, conversion coefficients, fluorescence yields, etc., were obtained from Nuclear Data Sheets[11] and the recent literature.[12,13] When necessary, correction was made for loss of photopeak intensity caused by summing with coincident γ rays. Decay curves were analyzed by a least-squares computer program[14] to give the activity at the end of irradiation. After correction for chemical yields (and other necessary corrections) the saturation activities were calculated. When combined with the Al monitor data and the foil weights, cross sections for production of these nuclides were obtained.

RESULTS

The cross sections for production of individual nuclides from silver irradiated by 3- and 29-GeV protons are listed in Table II. Values obtained in individual runs are given as well as the resulting mean values. Probable errors are 10–15% for most cases where at least two duplicate runs are available. Estimated accuracies of individual cases are discussed in footnotes to the Table. A (c) following the nuclide symbol indicates that the yield is cumulative and that at least one of the precursors is known; an (i) indicates that the yield is independent. In order to make the table as complete as possible, values have been included from other work, published as well as unpublished. The column headed σ_{29}/σ_3 lists the ratio of each nuclide cross section at 29 GeV to its value at 3 GeV.

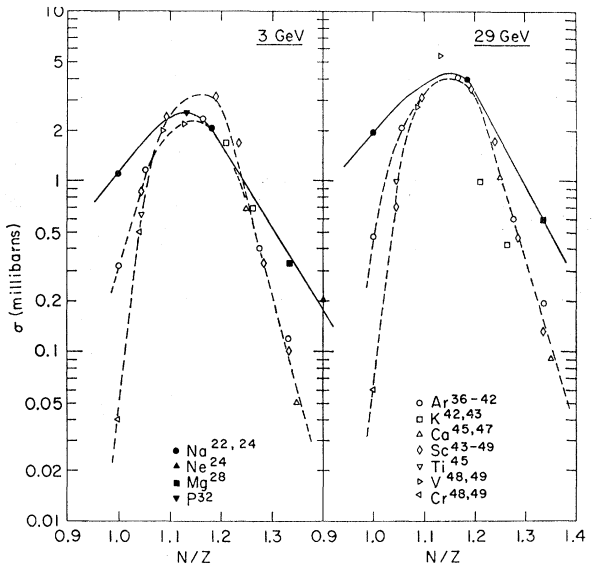

FIG. 1. Charge-distribution curves in the region of low mass products. The filled points and solid curves are for $A=22$–32; the open points and dashed curves are for $A=36$–49. Point symbols apply at both energies.

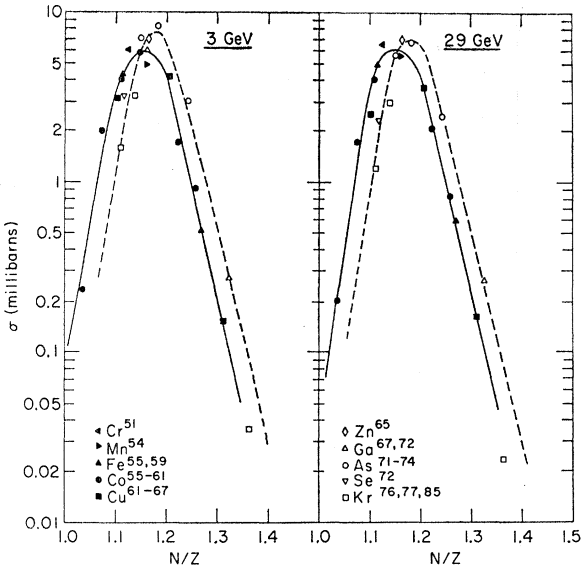

FIG. 2. Charge-distribution curves in the region of intermediate mass products. Filled points and solid curves are for $A=51$–67; open points and dashed curves are for $A=65$–85. Point symbols apply at both energies.

The nuclear charge distribution of the products in various mass regions can be obtained from the independent cross sections listed in Table II and from some of the other values which can be converted to independent cross sections by making small corrections. If at each bombarding energy it is assumed that within a

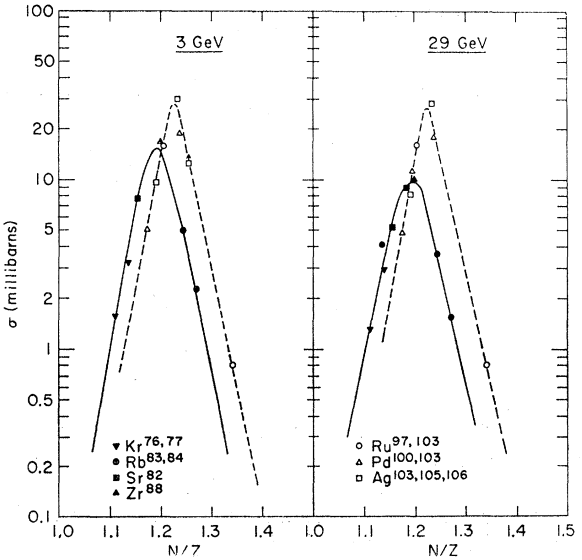

FIG. 3. Charge-distribution curves in the region of high mass products. Filled points and solid curves are for $A=76$–88; open points and dashed curves are for $A=97$–106. Point symbols apply at both energies.

[11] *Nuclear Data Sheets*, compiled by K. Way *et al.* (U. S. Government Printing Office, National Academy of Sciences—National Research Council, Washington, D. C.).

[12] *Nucl. Data* **1**, Sec. B (1966).

[13] C. M. Lederer, J. M. Hollander, and I. Perlman, *Table of Isotopes* (John Wiley & Sons, Inc., New York, 1967), 6th ed.

[14] J. B. Cumming, in *Application of Computers to Nuclear and Radiochemistry*, edited by G. D. O'Kelley (Office of Technical Services, Washington, D. C., 1963), NAS—NS 3107.

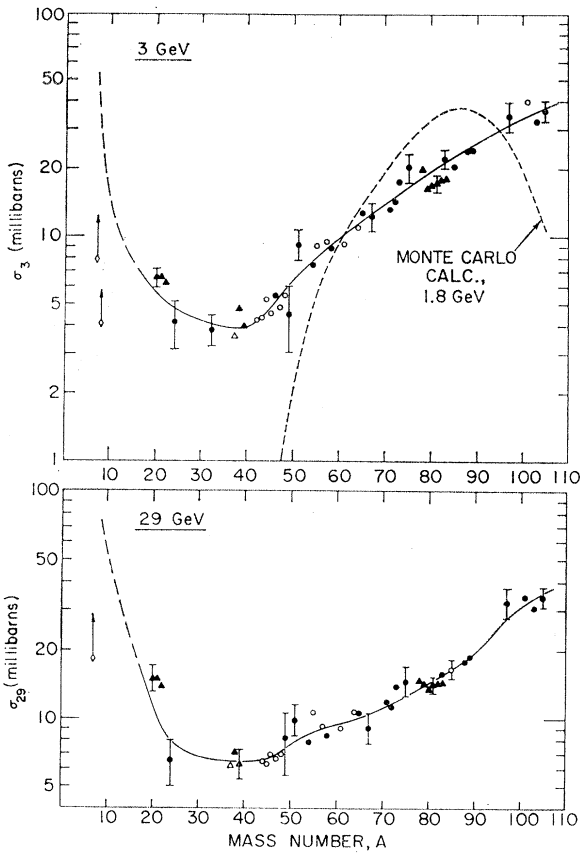

FIG. 4. Total isobaric cross sections as a function of product mass number at 3 GeV and at 29 GeV. The circles show data from the present work; the triangles show the results from other investigations. Filled points indicate that >50% of the total yield was observed and <50% was estimated from charge-distribution curves. Open points indicate that 30–50% of the yield was observed. The open diamonds with arrows represent lower limits. The dashed curve is for a Monte Carlo cascade-evaporation calculation for Ag+(1.8-GeV protons).

limited mass region the total isobaric cross sections are roughly constant, charge-distribution curves as shown in Figs. 1–3 may be constructed. The points on these plots represent independent cross sections for the nuclides listed in the legends. Most of them lie near the smooth curves, although in a few cases it was necessary to draw more than one curve within a given mass region. The greatest uncertainty is in the group of lowest masses ($A=18$–32) where the independent yields estimated for the stable neon isotopes are high by about a factor of 2.

Total isobaric cross sections for about 40 mass numbers at 3 and 29 GeV were calculated from the data of Table II and the charge-distribution curves of Figs. 1–3. Each value is shown in Table III together with that portion of the cross section observed directly and that portion estimated from the charge-distribution curves. The estimates take into account the effect of mass variation on individual curves. When >50% of the total cross section has been observed the value is shown in boldface type; when only 30–50% has been observed, ordinary type is used. Approximate values are enclosed in parentheses, and in some cases only lower limits are shown. These results are plotted in Figs. 4

TABLE III. Total isobaric cross sections from bombardment of silver with 3- and 29-GeV protons, and the corresponding isobaric cross-section ratios σ_{29}/σ_3. When >50% of total cross section was observed this is indicated by boldface type. When <30% was observed this is shown by parentheses.

σ (3 GeV) Obs.	+ Est. =	Total	Mass No.	σ_{29}/σ_3	σ (29 GeV) Total	= Est. +	Obs.
8		>8	7		>18.2		18.2
4		>4	8				
1.05		>1.1	9				
2.3		>2.3	11				
0.20		>0.2	13				
0.18		>0.18	16				
0.99		>0.99	17				
1.43		>1.43	18				
6.5		**6.5**	20	**2.31**	**15**		15
6.5		**6.5**	21	**2.31**	**15**		15
6.1		**6.1**	22	**2.25**	**13.7**		13.7
2.24	1.9	**4.1**	24	**1.59**	**6.5**	2.4	4.1
0.33		>0.33	28				0.59
2.51	1.3	**3.8**	32				
0.32	2.8	(3.1)	36		(5.4)	4.9	0.47
1.21	2.4	3.6	37	1.69	6.2	4.0	2.15
4.7		**4.7**	38	**1.49**	**7.0**		7.0
2.7	1.2	**3.9**	39	**1.62**	**6.3**	1.8	4.5
0.41	3.5	(3.9)	41		(6.4)	5.8	0.63
1.79	2.4	4.2	42		(4.5)	3.3	1.18
1.58	2.7	4.3	43		(5.7)	4.1	1.64
2.34	2.9	5.2	44	1.23	6.4	3.3	3.09
1.39	3.1	4.5	45	1.38	6.2	4.1	2.11
3.12	2.3	**5.4**	46	1.28	6.9	3.5	3.44
1.72	3.1	4.8	47	1.38	6.6	4.8	1.79
2.36	3.0	5.4	48	1.28	6.9	3.6	3.25
2.75	1.7	**4.5**	49	**1.82**	**8.2**	1.8	6.44
6.49	2.6	**9.1**	51	**1.08**	**9.8**	2.6	7.15
2.47		>2.5	52				
4.90	2.5	**7.4**	54	**1.04**	**7.7**	2.2	5.55
4.47	4.5	9.0	55	1.18	10.6	5.4	5.16
2.3	7.1	(9.4)	56		(9.2)	7.4	1.8
4.35	5.0	9.4	57	0.98	9.2	4.9	4.31
5.80	3.0	**8.8**	58	**0.94**	**8.3**	2.8	5.51
0.52		>0.52	59		>0.63		0.63
1.89	7.0	(8.9)	60		(9.1)	7.1	2.05
4.2	**5.0**	9.2	61	0.98	9.0	5.4	3.60
4.1	6.8	10.9	64	0.97	10.6	7.0	3.57
10.35	2.2	**12.6**	65	**0.83**	**10.5**	1.8	8.71
8.30	3.9	**12.2**	67	**0.74**	**9.0**	2.3	6.65
8.12	5.0	**13.1**	71	**0.91**	**11.9**	5.6	6.32
12.0	2.2	**14.2**	72	**0.79**	**11.2**	1.8	9.39
16.2	1.2	**17.4**	73	**0.79**	**13.8**	0.9	12.9
3.01	12.3	(15.3)	74		(11.2)	8.8	2.43
19.0	1.3	**20.3**	75	**0.72**	**14.6**	1.1	13.5
1.8	19.3	(21.1)	76		(11.5)	10.1	1.4
3.8	17.7	(21.5)	77		(13.2)	9.8	3.4
11.1	8.8	**19.9**	78	**0.74**	**14.7**	5.8	8.9
12.6	3.6	**16.2**	79	**0.87**	**14.1**	2.4	11.7
16.6	0.2	**16.8**	80	**0.80**	**13.4**	0.2	13.2
17.0	0.4	**17.4**	81	**0.80**	**14.0**	0.4	13.6
17.7	0.0	**17.7**	82	**0.80**	**14.1**	0.0	14.1
22.0	0.1	**22.1**	83	**0.71**	**15.6**	0.5	15.1
2.26	20.6	(22.9)	84		>1.6		1.55
19.5	0.8	**20.3**	85	**0.81**	**16.4**	0.6	15.8
20.1	3.8	**23.9**	88	**0.74**	**17.8**	2.6	15.2
22.6	1.6	**24.2**	89	**0.77**	**18.6**	1.1	17.5
19.5	15.0	**34.5**	97	**0.94**	**32.4**	13.3	19.1
6.67	37.5	(44)	100		>5.6		5.63
16.2	24.1	40.3	101	0.85	**34.4**	21.0	13.4
28.1	4.4	**32.5**	103	**0.95**	**30.8**	4.0	26.8
30.1	6.2	**36.3**	105	**0.94**	**34.3**	5.9	28.4
12.4		>12.4	106				

TABLE IV. Summary of results on nuclear charge distribution for various mass regions. The data apply to both 3 and 29 GeV. A_m is the median mass for a given region; N/Z_p is the neutron/proton ratio for the most probable nuclear charge Z_p of A_m; $\Delta(N/Z)$ is the full width at half-maximum of the charge-distribution curve; ΔZ is the corresponding spread in Z; Z_{A_m} is the most stable nuclear charge[a] for A_m; and $Z_{A_m}-Z_p$ shows the displacement of the most probable charge from the most stable charge for A_m (positive values show neutron excess). Estimated uncertainties are: N/Z_p, ±0.01; Z_p, ±0.5%; $\Delta(N/Z)$, ±10%; ΔZ, ±0.13; $Z_{A_m}-Z_p$, ±0.2.

Mass region	A_m	N/Z_p	Z_p	$\Delta(N/Z)$	ΔZ	Z_{A_m}	$Z_{A_m}-Z_p$
22–32	27	1.13	12.7	0.190	1.14	12.9	0.2
36–49	43	1.15	20.0	0.156	1.45	20.1	0.1
51–67	59	1.15	27.4	0.114	1.45	27.0	−0.4
65–77	71	1.18	32.6	0.087	1.30	31.5	−1.1
76–88	82	1.19	37.4	0.080	1.36	35.8	−1.6
97–106	102	1.23	45.8	0.051	1.05	44.6	−1.2

[a] C. D. Coryell, Ann. Rev. Nucl. Sci. 2, 305 (1953).

and 5. In Table III the column headed σ_{29}/σ_3 gives ratios of total isobaric cross sections for the two bombarding energies. These are shown in the lower part of Fig. 5 plotted as a function of mass.

It is interesting to compare the results of measurements made with a Ge(Li) detector on old irradiated silver foils with the corresponding results obtained from NaI measurements on chemically separated samples. The silver foils were from several irradiations at each energy and they were 1.6–3.5 years old when the measurements were made. The Ge(Li) detector had a volume of 8 cm^3 and a resolution of 3.5 keV. All the γ-ray peaks of appreciable intensity (except one at 695 keV) were assigned to the following nuclides: 2.6-year Na^{22}, 303-day Mn^{54}, 267-day Co^{57}, 5.26-year Co^{60}, 245-day Zn^{65}, 120-day Se^{75}, 3.2-year Rh^{101}, and the two isomers of Rh^{102}. The cross sections calculated for Na^{22}, Mn^{54}, and Se^{75} agreed with the results on chemically separated samples to within 10% or better. For Co^{57} only approximate agreement was obtained because the two main peaks were insufficiently resolved from interfering γ rays. The results for Zn^{65} were ~80% high; thus there must be an interfering γ ray at 1116 keV. Both lines for Co^{60}, 1173- and 1332-keV, gave results in excellent agreement with each other but none of the chemically separated cobalt samples had sufficient intensity to show these Co^{60} peaks. No chemically separated Rh samples were available for comparison with the gross counting. The case of Rh^{102} is complicated because the decay scheme of the 206-day and 2.5-year (?) isomers have not been completely disentangled. Summarizing, it can be said that simple Ge(Li) detector techniques require further elaboration before chemical separations become unnecessary for this type of study.

DISCUSSION

A. Nuclear Charge

A careful comparison of the 3-GeV charge-distribution curves with the corresponding 29-GeV curves

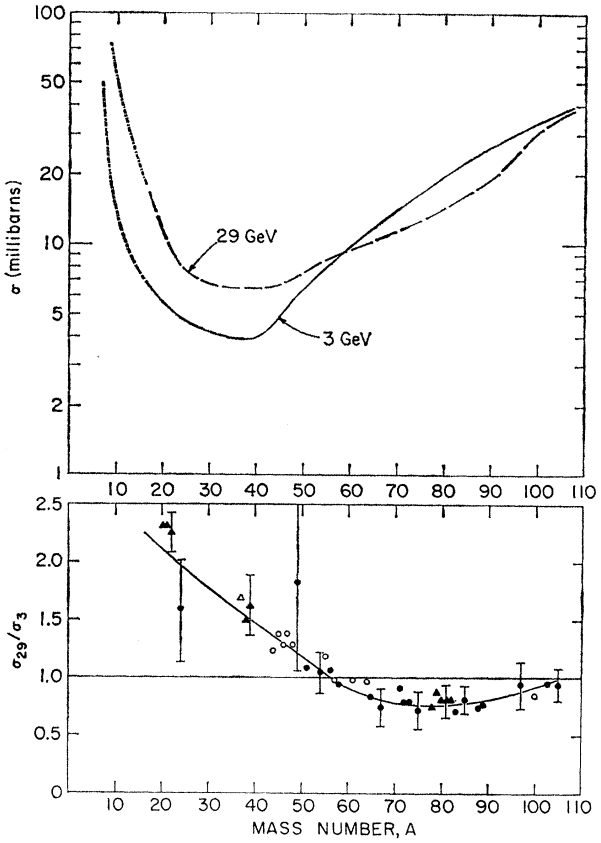

FIG. 5. Upper: Comparison of the mass-yield curves for Ag+(3-GeV protons) and Ag+(29-GeV protons). Lower: Ratio of total isobaric cross sections σ_{29}/σ_3 as function of product mass number; symbols have same meaning as in Fig. 4.

reveals that they are nearly identical in shape and in the N/Z values of the peaks. There is no evidence of any appreciable broadening of the curves when the bombarding energy is increased from 3 to 29 GeV.

Table IV summarizes some of the results of Figs. 1–3 and it contains additional derived quantities. In the calculation of these values corrections were applied, when necessary, for variation of the cross sections with mass number. The data apply to both bombarding energies. Column 1 gives the range of mass numbers within each group and column 2 shows the median mass A_m. Column 3 gives N/Z_p, the neutron/proton ratio at the peak of the charge-distribution curve. Values of Z_p, the most probable nuclear charge for A_m, are shown in column 4. The total widths of the curves at half-maximum and the corresponding ΔZ values are listed in columns 5 and 6, respectively. Although the curves of Figs. 1–3 get narrower with increasing A, the spread in Z at half-maximum, ΔZ, is almost constant at 1.4 charge units (except for the products which are close to, or very far from, the target). The charge of maximum stability Z_{A_m}, is shown in column 7. Finally, the last column lists $Z_{A_m}-Z_p$, the displacement of the most probable charge for a product of mass A_m from the

charge of maximum stability. Thus, the light products, $A<50$, tend to be formed, with greatest yield, at stability or very slightly to the neutron excess side. As the product mass increases the peak independent cross sections shift more and more to the neutron deficient side until at mass 82, $Z_{A_m}-Z_p=-1.6$. When the products are close to the target the peak is still on the neutron deficient side but somewhat closer to stability (e.g., at $A_m=102$, $Z_{A_m}-Z_p=-1.2$).

The charge dispersion of products in the mass region 65–72 from interaction of 2.9-GeV protons with indium was studied by Kaufman.[15] His published curve is almost identical with that found here for silver as the target. Porile and Church[16] have examined the isobaric yield distributions in the same region for targets of Zn^{96}, Mo^{96}, and Ru^{96} irradiated with 1.8-GeV protons. The curve for Mo^{96} is close to the one for silver or indium but the peak is 30% higher. As pointed out by these authors, the N/Z of the most probable product depends somewhat on the N/Z of the target. The three targets considered here differ little in N/Z: 1.285, 1.297, and 1.344 for Mo^{96}, natural Ag, and natural In, respectively.

B. Mass-Yield Distribution

The general shapes of the mass-yield curves for the 3- and 29-GeV irradiations, Fig. 4, are roughly similar to those found previously for copper,[7,17,18] tantalum,[4] and lead[3,6] targets. The yields are high for products close to the target, and then they decrease to a broad minimum at around one-third the target mass. The yields increase again for the very light products.

It is instructive to compare the 3-GeV experimental results with a calculation[19] based on the usual model of a fast nucleon cascade followed by particle evaporation. The Monte Carlo cascade calculations of Metropolis *et al.*[20] for 1.8-GeV incident protons were used to obtain a set of excited starting nuclei. Then the Monte Carlo evaporation method of Dostrovsky *et al.*[21] was applied to obtain the final distribution of product nuclei. The level-density parameter a was set equal to $(A/10)$ MeV^{-1}, and the nuclear radius parameter r_0 was taken as 1.5×10^{-13} cm. Particles up to mass 10 were considered in the calculation. The results are plotted as the dotted curve in Fig. 4. Although the calculated results are for a somewhat lower bombarding energy and the values chosen for the constants are subject to some variation, the main features of the comparison are valid. The agreement is reasonably good in the mass region 55–95. The shape of the calculated curve in this region can be expected to approach closer to that of the experimental curve if the calculations were made for 3-GeV protons. For products near to the target in mass, the calculation predicts cross sections that are too low. It is expected[22] that much, or all, of this deficit would be corrected by the use of a diffuse nuclear surface rather than a uniform nuclear-density distribution. For products below about mass 45, it is clear that the simple cascade-evaporation model gives cross sections that are much too small. By including in the calculation the emission of heavier fragments,[23,24] with $A>10$, residual nuclei of lower mass would also be produced, and the agreement with experiment in the mass 20–40 region would be improved. However, the energies and spins of all the excited states needed for such a calculation are not known.

Whatever the detailed mechanism is for production of nuclei in this region, the evidence indicates that a "two-body breakup" or "fission-like" process is involved. Studies of stars[25–29] in low-sensitivity nuclear emulsions show events in which two heavily ionizing particles produce dense tracks in roughly opposite directions. The most probable ratio of their ranges is unity. Furthermore, the observed range distribution[19] of these fragments corresponds, approximately, with that of Na^{24} product nuclei from the interaction of 2.9-GeV protons with silver. These range measurements were part of a radiochemical study[19] of the velocity and energy distributions of several products representing differing mass regions, i.e., Na^{24}, $Sc^{43,44}$, $Cu^{61,64}$, and Sr^{83}. The velocities of all of these, except Na^{24}, and marginally $Sc^{43,44}$, were found to be much lower than those of the heavily ionizing fragments seen in the binary emulsion events. These observations point to the identification of the light products, $A\approx15$–35, with both members of the emulsion binary events. The total integrated cross section at 3 GeV for products in the $A=15$–35 region is 108 ± 20 mb (Fig. 4). This is consistent with the value of 100 ± 20 mb found[27] for both of the heavily ionizing fragments of the "fission-like" events observed in nuclear emulsions irradiated at 2.9 GeV.

The total reaction cross section can be evaluated by summation of the isobaric yields in an appropriate manner. If we assume that all products of $A\leqslant25$ have partners of higher mass, we must simply add all the

[15] S. Kaufman, Phys. Rev. **129**, 1866 (1963).
[16] N. T. Porile and L. B. Church, Phys. Rev. **133**, B310 (1964).
[17] G. Friedlander, J. M. Miller, R. Wolfgang, J. Hudis, and E. Baker, Phys. Rev. **94**, 727 (1954).
[18] D. W. Barr, University of California Radiation Laboratory Report No. UCRL-3793, 1957 (unpublished).
[19] J. B. Cumming, S. Katcoff, N. T. Porile, S. Tanaka, and A. Wyttenbach, Phys. Rev. **134**, B1262 (1964); N. T. Porile (private communication).
[20] N. Metropolis, R. Bivins, M. Storm, J. M. Miller, G. Friedlander, and A. Turkevich, Phys. Rev. **110**, 204 (1958).
[21] I. Dostrovsky, Z. Fraenkel, and G. Friedlander, Phys. Rev. **116**, 683 (1959).
[22] K. Chen, Z. Fraenkel, G. Friedlander, J. R. Grover, J. M. Miller, and Y. Shimamoto, this issue, **166**, 949 (1968).
[23] I. Dostrovsky, R. Davis, Jr., A. M. Poskanzer, and P. L. Reeder, Phys. Rev. **139**, B1513 (1965).
[24] N. T. Porile, Phys. Rev. **141**, 1082 (1966).
[25] E. W. Baker and S. Katcoff, Phys. Rev. **123**, 641 (1961).
[26] E. W. Baker and S. Katcoff, Phys. Rev. **126**, 729 (1962).
[27] S. Katcoff, Phys. Rev. **164**, 1367 (1967).
[28] P. A. Gorichev, O. V. Lozhkin, and N. A. Perfilov, Zh. Eksperim. i Teor. Fiz. **45**, 1784 (1963) [English transl.: Soviet Phys.—JETP **18**, 1222 (1964)].
[29] P. A. Gorichev, O. V. Lozhkin, and N. A. Perfilov, Zh. Eksperim. i Teor. Fiz. **46**, 1897 (1964) [English transl.: Soviet Phys.—JETP **19**, 1276 (1964)].

isobaric cross sections for $A>25$. The results are 1270±150 mb for the 3 GeV proton irradiation and 1160±150 mb for the 29-GeV irradiation. These values are in excellent agreement with the geometric cross section of 1200 mb calculated for silver with $r_0=1.3\times10^{-13}$ cm and with the nuclear absorption cross section determined by Ashmore *et al.*[30]

The mass-yield curves at the two bombarding energies are compared in Fig. 5 (upper part). The ratio of isobaric cross sections, σ_{29}/σ_3, is plotted as a function of mass number in the lower part of Fig. 5. This ratio is about 2 at mass 20, and it decreases to about unity near mass 55. It then decreases more slowly to a very broad minimum of about 0.8 in the region of $A=70$–90, and finally it seems to rise again toward unity for products very near the target. Qualitatively, this behavior shows that events which require very high excitation become somewhat more probable at the higher bombarding energy, at the expense of events of more moderate excitation. This effect was barely noticeable when copper[7] was the target. However, for heavier elements,[6,31,32] such as Au, Pb, and U, the effect seems to be even more pronounced. As the beam energy is increased from 3 to 27 GeV the pion multiplicity observed[33] in nuclear emulsion stars increases sevenfold. Nearly all the additional pions escape from light target nuclei and thus do not deposit additional excitation energy. However, in heavier target nuclei there is appreciable probability for pion interaction and therefore there is some increase in the mean excitation energy.

There is a striking anomaly in the ratios of potassium isotope cross sections, σ_{29}/σ_3, at the two energies. The ratios are 0.59 and 0.66 for K^{42} and K^{43}, respectively (Table II), while for neighboring nuclides the σ_{29}/σ_3 ratios are about 1.4. It is improbable that this effect is due to experimental error because of the excellent agreement among replicate runs, each of which had duplicate samples. These samples were purified on columns of ammonium molybdophosphate and therefore were free of any Rb contamination. Potassium was also isolated in some earlier runs (not included in Table II) where the chemical separations gave samples which were not entirely free of contamination. The mean results were: K^{42}, 1.4 mb at 3 GeV, 1.1 mb at 29 GeV, ratio 0.8; K^{43}, 0.64 mb at 3 GeV, 0.47 mb at 29 GeV, ratio 0.7. The uncertainty in these early results is ±25% but they show the same trend as the later more accurate results. The low σ_{29}/σ_3 ratios for K^{42} and K^{43} arise mainly from low cross sections observed at 29 GeV for these isotopes. It seems unlikely that this is caused by diffusion of potassium out of the target during irradiation because the cross sections for Na, Rb, Ne, and Ar isotopes appear normal. Furthermore, the beam intensity in the different 29-GeV irradiations varied over an order of magnitude. No reasonable interpretation for this anomaly is now apparent.

SUMMARY AND CONCLUSION

The interaction of very-high-energy protons with silver results in the formation of product nuclei with all masses less than (or equal to) that of the target. The total isobaric cross sections at 3 GeV decrease from about 40 mb at mass 106 to about 4 mb at mass 35. Then they increase again for lighter products, reaching 6.5 mb at mass 20 and over 1000 mb at mass 4. For 29-GeV protons the cross sections are slightly lower for products relatively near to the target in mass, but substantially higher for products below mass 40. In both cases the total reaction cross section is about 1200 mb, close to geometric.

The isobaric charge distributions peak very close to stability for low mass products but for $A\geqslant60$ the most probable products are neutron deficient by 1–2 charge units. These charge distributions and N/Z values of the peaks are independent of beam energy between 3 and 29 GeV. The ΔZ corresponding to the full width at half-maximum of the charge-distribution curves is 1.4±0.1 charge units for all masses between 35 and 90.

The cascade-evaporation mechanism can account, at least approximately, for the cross sections of product nuclei down to about mass 50. It probably can be extended to include somewhat lower mass products by considering the evaporation of large fragments. However, the time scale for emission of such fragments and whether the process should be considered as evaporation or "fragmentation" are open questions.

The present investigation has been correlated with earlier nuclear emulsion work[25–29] and with radiochemical measurements[19] of the energy distributions of product nuclei. Direct measurement of fragment energies, velocities, and masses by counter techniques should greatly extend our knowledge of these high-energy nuclear reactions. New Monte Carlo cascade calculations, which take into account a diffuse nuclear surface and refraction effects[22] will allow more exact comparisons between theory and experiment.

ACKNOWLEDGMENTS

It is a pleasure to acknowledge the help of Charles G. Jameson, who assisted with the chemical separations and with the counting during the summer of 1965. We thank Dr. N. T. Porile for the calculated mass-yield curve shown in Fig. 4. To Dr. R. W. Stoenner and Dr. K. Rowley and to Miss E. Norton we are grateful for the numerous chemical-yield determinations.

[30] A. Ashmore, G. Cocconi, A. N. Diddens, and A. M. Wetherell, Phys. Rev. Letters **5**, 576 (1960).
[31] J. Hudis, T. Kirsten, O. A. Schaeffer, and R. W. Stoenner, Phys. Rev. (to be published).
[32] I. Dostrovsky and R. W. Stoenner (private communication).
[33] A. Barbaro-Galtieri, A. Manfredini, B. Quassiati, C. Castagnoli, A. Gainotti, and I. Ortalli, Nuovo Cimento **21**, 469 (1961).